Characterization of sulfur and nanostructured sulfur battery cathodes in electron microscopy without sublimation artifacts.

Barnaby D.A. Levin[1], Michael J. Zachman[1], Jörg G. Werner[2], Ritu Sahore[2], Kayla X. Nguyen[1], Yimo Han[1], Baoquan Xie[2], Lin Ma[2], Lynden Archer[3], Emmanuel P. Giannelis[2], Ulrich Wiesner[2], Lena F. Kourkoutis[1,4], David A. Muller[1,4]

1. School of Applied and Engineering Physics, Cornell University, Ithaca, NY, USA, 14853.
2. Department of Materials Science and Engineering, Cornell University, Ithaca, NY, USA, 14853.
3. School of Chemical and Biomolecular Engineering, Cornell University, Ithaca, NY, USA, 14853.
4. Kavli Institute for Nanoscale Science, Cornell University, Ithaca, NY, USA, 14853.

Abstract

Lithium sulfur (Li-S) batteries have the potential to provide higher energy storage density at lower cost than conventional lithium ion batteries. A key challenge for Li-S batteries is the loss of sulfur to the electrolyte during cycling. This loss can be mitigated by sequestering the sulfur in nanostructured carbon-sulfur composites. The nanoscale characterization of the sulfur distribution within these complex nanostructured electrodes is normally performed by electron microscopy, but sulfur sublimates and redistributes in the high vacuum conditions of conventional electron microscopes. The resulting sublimation artifacts render characterization of sulfur in conventional electron microscopes problematic and unreliable. Here, we demonstrate two techniques, cryogenic transmission electron microscopy (cryo-TEM) and scanning electron microscopy in air (airSEM),

that enable the reliable characterization of sulfur across multiple length scales by suppressing sulfur sublimation. We use cryo-TEM and airSEM to examine carbon-sulfur composites synthesized for use as Li-S battery cathodes, noting several cases where the commonly-employed sulfur melt infusion method is highly inefficient at infiltrating sulfur into porous carbon hosts.

Introduction

Lithium sulfur (Li-S) batteries have the potential to provide greater energy storage density at lower cost than current lithium ion batteries. One of the main challenges to improving the performance of elemental sulfur cathodes for Li-S batteries is dissolution and loss of sulfur, in the form of polysulfides, to the electrolyte during battery operation (Bruce et. al., 2011). Recent research has focused on electrodes which attempt to sequester sulfur in nanostructured host materials, most prominently porous carbons, to prevent the loss of sulfur and associated capacity reduction as the battery is cycled (Ji et. al., 2009; Jayaprakash et. al., 2011; Wang et. al. 2011; Xiao et. al., 2012; Seh et. al. 2013; Zheng et. al., 2013; Song et. al., 2014; Zhao et. al., 2014; Werner et. al., 2015; Sahore et. al. 2015). These electrode materials are typically referred to as carbon-sulfur composites. Accurate characterization of the distribution of sulfur in these composites over 100 nm to sub-nm length scales is critical for developing an understanding of how the level of infiltration of sulfur into the host material relates to battery performance, which will aid in the design of more durable, high energy density Li-S batteries (Ma et. al. 2015).

Electron microscopy offers both direct imaging and spectroscopic techniques for characterization of battery electrodes. For reliable characterization of a material using electron microscopy, it is essential that the sample is not altered by conditions in the microscope. However, elemental sulfur readily sublimates under high vacuum conditions similar to those of an electron microscope sample chamber. Sulfur sublimation under high vacuum has been observed in vacuum

chamber experiments on bulk sulfur (Nash, 1987), and can be predicted from sulfur's measured vapor pressure (Ferreira & Lobo, 2011), but the sulfur battery community has only recently begun to become aware of the problem of sulfur sublimation in electron microscopy (Raiβ et. al., 2014). As an illustration of this challenge, Figure 1a shows the vapor pressure curve of sulfur, with the conditions of an FEI Tecnai F20 transmission electron microscopy (TEM) sample chamber (8.8×10^{-8} Torr at ~ 18ºC room temperature) indicated. Figures 1b-g show the result of placing a sample of ball-milled sulfur particles into the microscope under these conditions. The sulfur is observed to sublimate at a rate of approximately 1 monolayer of sulfur atoms per second, leaving behind only a small residue of "super-sublimated" polymeric sulfur, which remains relatively stable under vacuum. The measured sublimation rate and residual product are fully consistent with previous macroscopic experiments (Nash, 1987).

In nanostructured sulfur composites, sublimation effects in high vacuum may be very severe. In TEM for example, exposed nanoscale features of the sulfur distribution in a sulfur battery cathode composite would disappear within minutes at most. Only super-sublimated polymeric sulfur residue (Figure 1e), and sulfur encapsulated by another material lacking large enough pores for sulfur to escape (Zhou et. al., 2014; Kim et. al., 2015), will remain present under vacuum.

In scanning electron microscopy (SEM), the sample is typically held at a higher pressure than in TEM. However, a recent study has observed that even in the vacuum of an SEM sample chamber (~ 10^{-6} Torr), sulfur sublimation artifacts occur, including the redistribution of sublimated sulfur into the pores of nearby carbon particles. The study concluded that characterization of sulfur/carbon composite materials by vacuum-based methods, including SEM, is very challenging, and results might be misleading (Raiβ et. al., 2014). Sulfur sublimation and the resulting artifacts,

including sulfur redistribution, present a serious problem for accurate characterization of the inherent sulfur distribution in battery cathodes in electron microscopy. This may be impeding the scientific community's efforts to gain a systematic understanding of how sulfur distribution in different carbon-sulfur composites relates to their performance in batteries. More reliable alternative techniques for sulfur characterization that suppress sublimation are clearly needed.

The sulfur vapor pressure curve (Figure 1a) indicates that sulfur has an equilibrium vapor pressure of ~ 6×10^{-7} Torr at 18°C. This means that at 18°C, a sulfur particle will sublimate until the partial pressure of sulfur surrounding the particle reaches 6×10^{-7} Torr. If a sample chamber is pumped to too low a pressure, sulfur will not be able to reach equilibrium, and will sublimate continually. To avoid sublimation artifacts, either the ambient pressure during imaging must be increased to a level much greater than sulfur's equilibrium vapor pressure, or the ambient temperature must be reduced to much less than 18°C. In this paper, we demonstrate characterization of sulfur and nanostructured carbon-sulfur composite materials in vacuum at low temperature using cryo-TEM, and at atmospheric pressure at room temperature using airSEM. Sulfur sublimation artifacts are not observed using either technique. Our results demonstrate that sulfur infiltration by melt infusion is significantly more efficient in activated porous carbons than in non-activated porous carbons, carbon nanotubes, and hollow carbon spheres, all of which have recently been investigated as Li-S battery electrode materials. Adoption of cryo-TEM, airSEM, and other similar techniques, for more reliable characterization of the sulfur distribution in different carbon-sulfur composites will enable scientists to observe the inherent sulfur distribution in their composite materials, providing important insight and feedback to guide the design of improved Li-S batteries.

Experimental

Cryo-TEM is a well-established method for imaging hydrated biological samples that cannot be exposed to vacuum at room temperature (Dubochet & McDowall, 1981; Adrian et. al., 1984; Kourkoutis et. al. 2012). Cryogenic cooling of sulfur cathode samples inside the microscope was achieved using a Gatan model 626 cryo-holder (Gatan, Inc., Pleasanton, CA, USA), with liquid nitrogen as the cryogen. The cryo-TEM loading method for sulfur cathode samples is simpler than for biological samples, since the sulfur need only be cooled prior to loading into the microscope column, whereas biological samples must be vitrified. Carbon-sulfur composite particles were dispersed from an ethanol solution onto TEM grids, which were then allowed to dry in air. The cryo-holder was cooled so that the tip temperature was ~ -173^{o}C. The sample TEM grids were loaded into the cryo-holder under nitrogen gas near liquid nitrogen temperature. An FEI Tecnai F20 STEM/TEM (FEI Company, Hillsboro, OR, USA) equipped with cryogenically cooled beryllium blades, and operated in scanning TEM (STEM) mode at 200 kV was used to image the samples. An Oxford Instruments XMAX detector (Oxford Instruments PLC, Tubney Woods, Oxfordshire, UK) was used for x-ray energy dispersive spectroscopy (XEDS), and a Gatan 865 HR-GIF spectrometer was used for electron energy loss spectroscopy (EELS) acquisition.

Experiments in air were performed using a B-nano airSEM (B-nano Ltd. Rehovot, Israel), operated at 30 kV. The airSEM is a relatively new design of electron microscope (a schematic diagram of an airSEM is shown in Supplementary Figure S1), which enables characterization of samples in air, with no sample vacuum chamber (Nguyen et. al., 2013; Solomonov et. al., 2014; Vidavsky et. al. 2014; Nguyen et. al., 2016). Carbon-sulfur composite particles for analysis in airSEM were dispersed onto TEM grids from an ethanol solution and allowed to dry in air, in the same manner as for cryo-TEM. Sample TEM grids were placed directly on top of an airSTEM detector (Nguyen et. al., 2014; Han et. al. 2015; Nguyen et. al., 2016), which was mounted on an

optical slide. A white light optical reflectance microscope (Olympus, Centre Valley, PA, USA) was used both for optical imaging, and to set the height of the sample to ~ 50 μm below the electron window, the optimal working distance for airSEM imaging. XEDS maps were acquired using a Bruker XFlash 6160 detector (Bruker Corporation, Billerica, MA, USA).

Pure sulfur particles were prepared for analysis by ball-milling sulfur flakes. Carbon-sulfur composites synthesized with ordered mesoporous carbon structures GDMC-15-1600°C and aGDMC-15-10h, were obtained from block copolymer co-assembly and heated to 1600ºC to remove any intrinsic microporosity. The high-temperature treatment yielded low oxygen content and surface functionalization (hydrophobic surface). Carbon aGDMC-15-10h underwent activation by heating in CO_2 at 950ºC for 10 hours. Sulfur infiltration by melt infusion was attempted at a sulfur:carbon ration of 1:1 by weight. The synthesis, and performance of these mesoporous materials in battery testing is described in detail by Werner et. al. (Werner et. al., 2015). Carbon nanotube – sulfur composite samples, CNT-S, were synthesized using multi-walled, > 8% carboxylic acid functionalized carbon nanotubes, average diameter ~ 9.5 nm, length ~ 1.5 μm, which were obtained from Sigma Aldrich, and dried before use. Polyethylenimine (PEI) solution (50 wt. % in water) was obtained from Sigma-Aldrich, and PEI was covalently grafted to the carbon nanotubes. Sulfur infiltration by melt infusion was then attempted at a sulfur:carbon ration of 7:3 by weight. Mesoporous hollow carbon sphere – sulfur composites, MHCS-S, were prepared by an organic hard template method. In a typical synthesis, size tunable mono-dispersed melamine-formaldehyde (MF) resin sphere templates (0.5 g) were synthesized by the in-situ polymerization method reported by Xie et al. (Xie et al., 2008). These were then suspended in a 50 mL water/ethanol (volume ratio 3/1) solvent containing 0.5 g of Triton X-100 surfactant. Formaldehyde solution (1.0 mL) and resorcinol (0.75 g) were then added to the reaction solution,

and stirred for 30 min at 60°C. The solution was subsequently heated for 2 hours at 75°C. The solid product was recovered by filtration and air-dried at 90°C for 8 hours. Mesoporous hollow carbon spheres were formed by carbonization of the as-made resorcinol-formaldehyde encapsulated MF spheres at 950°C for 2 hours under flowing nitrogen gas with a heating rate of 3°C/min. Sulfur infiltration was attempted by melt infusion at a sulfur:carbon ratio of 7:3 by weight.

Results and Discussion

I. Sulfur characterization in cryo-TEM.

In order to investigate whether sublimation effects were still apparent at cryogenic temperatures, ball milled sulfur particles, were prepared in an identical manner to those in Figure 1, and imaged by cryo-TEM at a temperature of approximately -173°C. A time series of cryo-TEM images from a sulfur particle is shown in Figure 2. No change in the morphology of the particle was observed over a 5-hour period, in stark contrast to the sulfur particle imaged by standard room temperature TEM shown in Figure 1, which sublimated and disappeared in under 40 minutes. The cryogenically cooled sulfur remained stable enough under the electron beam to allow imaging in annular dark field (ADF) cryo-scanning TEM (cryo-STEM, Figure 2d) and XEDS mapping (Figure 2e). The suppression of sulfur sublimation by cryogenic sample cooling demonstrates that cryo-TEM is a viable method for both imaging and spectroscopic characterization of composites containing elemental sulfur such as carbon-sulfur nanocomposites for advanced lithium batteries.

Having established that sulfur sublimation is suppressed at cryogenic temperatures, we used cryo-TEM to analyze the sulfur distribution within three different carbon-sulfur nanocomposite materials recently investigated for Li-S battery electrodes. The first two samples, GDMC-15-1600°C and aGDMC-15-10h, are examples of ordered carbon nano-networks (Werner

et. al., 2015). These have attracted interest as sulfur battery cathode materials due to the potential of sequestering sulfur in the pores of a torturous carbon network. GDMC-15-1600°C and aGDMC-15-10h were prepared in an identical manner except that, prior to sulfur melt infusion, aGDMC-15-10h underwent an additional activation procedure to substantially increase its microporosity and associated surface area, whereas the non-activated carbon, GDMC-15-1600°C, exhibits very little microporosity (see Experimental). The third sample, CNT-S used a network of carbon nanotubes as the host material for sulfur. Carbon nanotubes have attracted interest as Li-S battery electrodes due to the potential to sequester sulfur inside the body of the nanotubes (Fujimori et. al., 2013; Kim et. al., 2015). In each of our three samples, successful melt infusion would ensure that electrically insulating sulfur is in contact with electrically conducting carbon at the nanoscale. Cryo-STEM imaging and XEDS maps of the activated C-S composite aGDMC-15-10h (Figure 3a), showed a high degree of infiltration of sulfur into the carbon following melt infusion. However, in the non-activated C-S composite GDMC-15-1600°C we observed that a majority of the sulfur had not infiltrated the carbon, and remained external to the carbon particles (Figure 3b). External sulfur particles typically had a diameter of several μm or larger. In reported battery performance tests, the activated carbon aGDMC-15-10h outperformed its non-activated counterpart GDMC-15-1600°C in terms of initial capacity, capacity retention over cycling, and rate capability (Werner et. al., 2015). This may be partly explained by our observation that sulfur infiltration was much more successful in the activated carbon aGDMC-15-10h than the non-activated carbon GDMC-15-1600°C, because the external sulfur particles observed in GDMC-15-1600°C would be in poorer electrical contact with the carbon, and more exposed to dissolution and loss to the electrolyte in the form of polysulfides during battery cycling.

High magnification STEM imaging and EELS spectra of sample CNT-S indicated that little or no sulfur had infiltrated into the carbon nanotubes, which had remained hollow (Figure 3c). XEDS mapping of sample CNT-S at low magnification showed that much of the sulfur in the composite remained external to the nanotube network after melt infusion, forming particles several microns in diameter (Figure 3d), in a similar way to the sulfur in sample GDMC-15-1600°C. X-ray sum spectra from the datasets used to generate element distribution maps contain information about the relative quantities of carbon and sulfur in the field of view that are not evident from x-ray maps alone. The x-ray spectra used to generate the maps in Figure 3 are shown in Supplementary Figure S2. Each of these spectra show a strong sulfur peak relative to the carbon peak, indicating significant quantities of sulfur in the field of view. Our results show that the degree to which sulfur infiltrates into carbon host particles can vary significantly depending on the porosity and structural characteristics of the carbon host, and how the carbon was prepared. In this case, sulfur infiltrated far more efficiently into the activated, high-surface area carbon aGDMC-15-10h exhibiting both 15 nm mesopores and a large fraction of small micropores (< 4 nm), than into the non-activated carbon GDMC-15-1600°C, exhibiting only 15 nm mesopores, or into a network of carbon nanotubes. In a related cryo-TEM study of sulfur infusion into highly porous carbons synthesized by ice templation, sulfur was observed to have infiltrated far more efficiently into activated carbon 20-2-1.5-80S exhibiting both mesopores and micropores, than into non-activated carbon 20-2-0-80S, exhibiting only mesopores (Sahore et. al., 2016), a very similar trend to the results described above.

II. Sulfur characterization in airSEM.

An alternative approach to cryogenic cooling to avoid sulfur sublimation is to keep the sample at room temperature, but increase the pressure around the sample, for example by imaging

the sulfur at atmospheric pressure. The recently developed airSEM by B-nano enables correlative optical and electron microscopy of samples in air, with no vacuum specimen chamber, by using an electron transparent silicon-nitride window to separate the sample in air from the electron optics in vacuum (Solomonov et. al., 2014; Vidavsky et. al. 2014; Nguyen et. al., 2016). Our cryo-TEM observations of external sulfur particles several μm in diameter in carbon-sulfur composite samples suggested that correlative optical-electron microscopy would be a useful method of high-throughput characterization of these materials. Optical microscopy can screen samples for large external sulfur particles, since external sulfur (yellow) is optically distinct from carbon (black). Electron microscopy and XEDS can then be used to image carbon particles at higher magnification to analyze the degree of sulfur infiltration into the carbon, and investigate nanoscale features of the sulfur distribution.

As a demonstration of this technique, we used airSEM to investigate the distribution of sulfur in sample MHCS-S, a composite of sulfur and 3 μm diameter hollow carbon spheres with porous shells. These have attracted interest as candidate materials for Li-S batteries because of the potential for large quantities of sulfur to be sequestered in both the porous shell, and in the hollow interior of the sphere, though some recent studies have questioned whether melt infusion is actually successful at infiltrating sulfur into the hollow interior (Jayaprakash et. al., 2011; He et. al., 2013). In our sample, sulfur infiltration was attempted by melt infusion at a ratio of 7:3 sulfur to carbon by weight prior to imaging, sufficient to ensure that both the pores in the shell wall, and the interior cavity could be filled if melt infusion was successful.

Particles of external sulfur were identified by optical microscopy (Figure 4a). Closer inspection of a ~ 30 μm wide external sulfur particle (Figure 4b) with airSEM, using a bright-field STEM detector positioned directly below the sample (Nguyen et. al., 2014; Han et. al. 2015;

Nguyen et. al., 2016), shows a morphology that suggests this particle was formed by freezing from a liquid state. XEDS mapping confirmed the identity of the particle as external sulfur (Figure 4c & 4d, spectrum in Supplementary Figure S4a). Clusters of carbon spheres were identified in the optical microscope (Figure 4e) and imaged at high resolution in the airSEM (Figure 4f). The spheres appeared to be unfilled in the airSEM images, suggesting that sulfur had not infiltrated into the sphere interior. This was confirmed by XEDS mapping (Figure 4g & 4h, spectrum in Supplementary Figure S4b). However, XEDS maps did show that sulfur had infiltrated the walls of the spheres, despite not infiltrating the hollow interior as had been intended.

III. Comparison of airSEM and cryo-TEM

The spatial resolution set by electron optics in the airSEM will be more limited than for cryo-TEM. However, an advantage of the airSEM is that samples do not need to be cooled and placed in a vacuum chamber, meaning that airSEM can achieve greater sample throughput. AirSEM will be most suitable for use in conjunction with optical microscopy for high-throughput characterization of samples using a broader field of view where image resolution of < 5 nm is not required, whereas cryo-TEM will be most suitable for characterization of samples that require resolution of finer, nanometer scale features.

IV. Limitations due to radiation damage

Even after sublimation has been suppressed, radiation damage will ultimately limit the resolution at which sulfur can be characterized in electron microscopy. Electrical insulators, such as sulfur, are vulnerable to ionization damage (Egerton & Malac, 2004). Furthermore, sulfur molecules are weakly bound, making sulfur vulnerable to knock-on displacement damage (Chisney et. al., 1988). When sulfur is imaged at relatively low magnification, as in the results

presented in this paper, electron dose is spread over a wide area, and beam damage effects to sulfur will be minimal. However, at high magnification, electron dose becomes more concentrated and radiation damage will cause mass loss from sulfur particles. Radiation damage effects have been observed in Supplementary Figure S5, which is accompanied by further discussion of damage.

Conclusions

The high vapor pressure of sulfur creates a serious risk that sublimation artifacts will lead to a mischaracterization of samples containing sulfur in standard high-vacuum electron microscopy. As a solution to this problem, we have demonstrated that sulfur sublimation is suppressed by cooling sulfur samples below the sulfur sublimation point in vacuum using cryo-TEM, or by using airSEM to image sulfur in air. Both techniques are able to detect features of the sulfur distribution across C-S nanocomposite materials that are extremely challenging to observe reliably in standard electron microscopy due to sulfur sublimation in vacuum and resulting artifacts such as sulfur redistribution. Most notably, in three of the four carbon-sulfur composite samples investigated in this paper, we have directly observed that sulfur infiltration by melt infusion is unsuccessful or inefficient, leaving much of the sulfur external to the carbon host material. It may be of interest for future studies to investigate whether inefficient sulfur infiltration by melt infusion occurs in other composite materials, and to what extent this affects battery performance.

In conclusion, we strongly recommend adoption of cryo-TEM, airSEM for more reliable characterization of sulfur and sulfur battery cathodes. Other techniques that may also be able to suppress sulfur sublimation artifacts could include environmental SEM, cryo-SEM, and environmental-cell TEM. Applying these techniques to Li-S batteries will allow researchers to reliably characterize the inherent distribution of sulfur in their composite electrodes, helping to guide the design of improved lithium sulfur batteries.

Acknowledgements

This project was supported by the Energy Materials Centre at Cornell, an Energy Frontier Research Centre funded by the U.S. Department of Energy, Office of Science, BES Award DE-SC0001086; and the New York State Centre for Future Energy Systems (CFES), a joint Center for Advanced Technology between Cornell University and Rensselaer Polytechnic Institute, supported by the New York State, Empire State Development Division of Science, Technology and Innovation (NYSTAR), under contract number C100126.

This work made use of the Cornell Centre for Materials Research Shared Facilities which are supported through the NSF MRSEC program (DMR-1120296). The authors thank John Grazul for assistance in the TEM facilities.

References

Adrian, M., Dubochet, J., Lepault, J., & McDowall, A.W., (1984) Cryo-electron microscopy of viruses. *Nature*, **308**, 32-36.

Bruce, P. G., Freunberger, S. A, Hardwick L.J., & Tarascon, J.M., (2011) Li–O2 and Li–S batteries with high energy storage. *Nature Materials*, **11** (1) 19–29.

Chisney, D.B., Boring, J.W., Johnson, R.E. & Phipps, J.A. (1988), Molecular ejection from low temperature sulfur by keV ions. *Surface Science*, **195**, 594-618.

Dubochet, J., & McDowall, A.W., (1981) Vitrification of pure water for electron microscopy. *Journal of Microscopy*, **124** RP3–RP4.

Egerton, R.F., Li, P. & Malac, M., (2004) Radiation damage in the TEM and SEM, *Micron* **35**, 399–409.

Ferreira, A.G.M., & Lobo, L.Q., (2011) The low-pressure phase diagram of sulfur. *J. Chem. Thermodynamics*, **43**, 95-104.

Fujimori, T., Morelos-Gómez, A., Zhu, Z., Muramatsu, H., Futamura, R., Urita, K., Terrones, M., Hayashi, T., Endo, M., Hong, S.Y., Chul Choi, Y., Tománek, D., Kaneko, K., (2013) Conducting linear chains of sulphur inside carbon nanotubes, *Nature Communications*, **4**, 2162.

Han, Y.; Nguyen, K., Ogawa, Y., Shi, H., Park, J. & Muller, D. A. (2015) Electron Microscopy in Air: Transparent Atomic Membranes and Imaging Modes, *Microscopy and Microanalysis*, **21** (S3) 1111-1112

He, G., Evers, S., Liang, X., Cuisinier, M., Garsuch, A. & Nazar, L.F., (2013) Tailoring Porosity in Carbon Nanospheres for Lithium–Sulfur Battery Cathodes, *ACS Nano*, **7**, 10920-10930.

Jayaprakash, N., Shen, J., Moganty, S.S., Corona, A., & Archer, L.A., (2011) Porous Hollow Carbon-Sulfur Composites for High-Power Lithium–Sulfur Batteries. *Angewandte Chemie*, **123**, 6026–6030.

Ji, X., Lee, K.T., & Nazar, L.F. A highly ordered nanostructured carbon–sulphur cathode for lithium–sulphur batteries. (2009) *Nature Materials*, **8**, 500 – 506.

Kim, H., Lee, J. T., Magasinski, A., Zhao, K., Liu, Y. & Yushin, G., (2015) In Situ TEM Observation of Electrochemical Lithiation of Sulfur Confined within Inner Cylindrical Pores of Carbon Nanotubes *Adv. Energy Mater.*, **5**, 1501306.

Kourkoutis, L.F., Plitzko, J.M., & Baumeister, W., Electron microscopy of biological materials at the nanometer scale. (2012) *Annual Review of Materials Research*, **42**, 33–58.

Ma, L., Hendrickson, K.E., Wei, S., & Archer, L.A. (2015) Nanomaterials: Science and applications in the lithium-sulfur battery. *Nano Today*, **10**, 315-338.

Nash, D.B. (1987) Sulfur in vacuum: Sublimation effects on frozen melts, and applications to Io's surface and torus. *Icarus*, **72**, 1-34.

Nguyen, K.X. Holtz, M.E. & Muller, D.A. (2013) AirSEM: Electron Microscopy in Air, without a Specimen Chamber *Microscopy and Microanalysis,* **19**, (S2), 428-429.

Nguyen, K.X., Holtz, M.E., Richmond-Decker, J., Milstein, Y., & Muller, D.A., (2014) Spatial Resolution of Scanning Electron Microscopy without a Vacuum Chamber, *Microscopy and Microanalysis* **20**, (S3), 26-27.

Nguyen, K.X., Holtz, M.E., Richmond-Decker, J. & Muller, D.A., (2016) Spatial Resolution in Scanning Electron Microscopy and Scanning Transmission Electron Microscopy, Without a Specimen Vacuum Chamber, *Microscopy and Microanalysis,* Doi:10.1017/S1431927616011405

Raiβ, C., Peppler, K., Janek, J., & Adelhelm, P. (2014) Pitfalls in the characterization of sulfur/carbon nanocomposite materials for lithium–sulfur batteries. *Carbon,* **79**, 245-255.

Sahore, R., Estevez, L.P., Ramanujapuram, A., DiSalvo, F.J. & Giannelis, E.P. (2015) High-rate lithium–sulfur batteries enabled by hierarchical porous carbons synthesized via ice templation. *Journal of Power Sources*, **297**, 188-194.

Sahore, R., Levin, B. D. A., Muller, D. A., DiSalvo, F. J. & Giannelis, E. P., (2016) Design Principles for Optimum Performance of Porous Carbons in Lithium–Sulfur Batteries, *Adv Energy Mater* **6**, 1600134.

Seh, Z.W., Li, W., Cha, J. J., Zheng, G., Yang, Y., McDowell, M.T., Hsu, P.C., & Cui, Y. (2013) Sulphur–TiO_2 yolk–shell nanoarchitecture with internal void space for long-cycle lithium–sulphur batteries. *Nature Communications*, **4**, 1331.

Solomonov, I., Talmi-Frank, D., Milstein, Y., Addadi, S., Aloshin, A., & Sagi, I., (2014), Introduction of correlative light and airSEMTM microscopy imaging for tissue research under ambient conditions. *Nature Scientific Reports*, **4**, 5987.

340 Song, J., Xu, T., Gordin, M.L., Zhu, P., Lv, D., Jiang, Y.B., Chen, Y., Duan, Y., & Wang, D.,
341 (2014) Nitrogen-Doped Mesoporous Carbon Promoted Chemical Adsorption of Sulfur and
342 Fabrication of High-Areal-Capacity Sulfur Cathode with Exceptional Cycling Stability for
343 Lithium-Sulfur Batteries. *Advanced Functional Materials*, **24**, 1243–1250.
344 Vidavsky, N., Addadi, S., Mahamid, J., Shimoni, E., Ben-Ezra, D., Shpigel, M., Weiner, S., &
345 Addadi, L., (2014), Initial stages of calcium uptake and mineral deposition in sea urchin embryos.
346 *Proc. Natl. Acad. Sci. USA*. **111** (1), 39–44.
347 Wang, H., Yang, Y., Lian, Y., Robinson, J.T., Li, Y., Jackson, A., Cui, Y., & Dai, H. Graphene-
348 Wrapped Sulfur Particles as a Rechargeable Lithium–Sulfur Battery Cathode Material with High
349 Capacity and Cycling Stability. (2011) *Nano Letters*, **11** (7), 2644–2647.
350 Werner, J.G., Johnson, S.S., Vijay, V., & Wiesner, U. (2015) Carbon–Sulfur Composites from
351 Cylindrical and Gyroidal Mesoporous Carbons with Tunable Properties in Lithium–Sulfur
352 Batteries. *Chem. Mater*, **27**, 3349-3357.
353 Xiao, L., Cao, Y., Xiao, J., Schwenzer, B., Engelhard, M.H., Saraf, L.V., Nie, Z., Exarhos, G. J.,
354 & Liu, J., (2012) A Soft Approach to Encapsulate Sulfur: Polyaniline Nanotubes for Lithium-
355 Sulfur Batteries with Long Cycle Life. *Advanced Materials*, **24**, 1176–1181.
356 Xie, B., Shi, H., Liu, G., Zhou, Y., Wang, Y., Zhao, Y., Wang, D., (2008) Preparation of surface
357 porous microcapsules templated by self-assembly of nonionic surfactant micelles. *Chem. Mater.*,
358 **20**, (9), 3099-3104.
359 Zhao, Y., Wu, W., Li, J., Xu, Z., & Guan, L. (2014), Encapsulating MWNTs into Hollow Porous
360 Carbon Nanotubes: A Tube-in-Tube Carbon Nanostructure for High-Performance Lithium-Sulfur
361 Batteries. *Advanced Materials*, **26**, p. 5113-5118.

Zheng, G., Zhang, Q., Cha, J.J., Yang, Y., Li, W., Seh, Z. W., & Cui, Y., (2013) Amphiphilic Surface Modification of Hollow Carbon Nanofibers for Improved Cycle Life of Lithium Sulfur Batteries. *Nano Letters*, **13** (3), 1265–1270.

Zhou, W., Xiao, X., Cai, M., & Yang, L. (2014) Polydopamine-Coated, Nitrogen-Doped, Hollow Carbon−Sulfur Double-Layered Core−Shell Structure for Improving Lithium−Sulfur Batteries *Nano Letters*, **14**, 5250−5256.

Figures

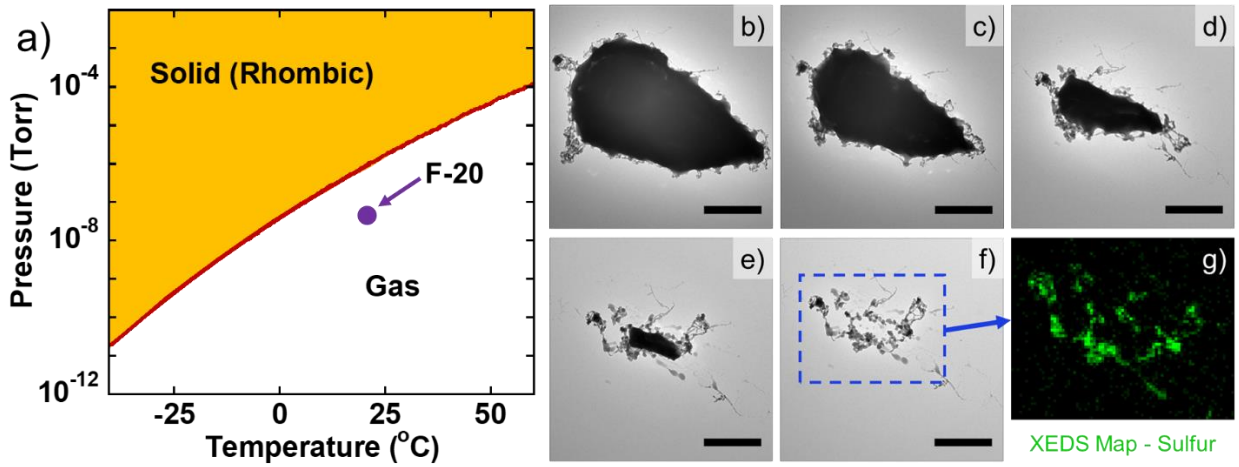

Figure 1. a) Vapor pressure vs temperature for elemental sulfur (Ferreira & Lobo, 2011). Purple marker indicates approximate conditions in specimen chamber of the F20 TEM used for image acquisition. **b) – f)** Sulfur particle sublimating in TEM vacuum chamber at 18°C, at a pressure of 8.8×10^{-8} Torr, imaged after (b) 16 min, (c) 21 min, (d) 28 min, (e) 33 min, (f) 40 min under vacuum. Scale bars 1µm. The particle was not exposed to the electron beam between images. After 40 min, particle has sublimated almost completely, leaving a small residue, which was stable in vacuum. STEM-XEDS map **(g)** indicates that the residue is sulfur. Residue morphology suggests the formation of super-sublimated polymeric sulfur, as expected from the macroscopic experiments of (Nash, 1987).

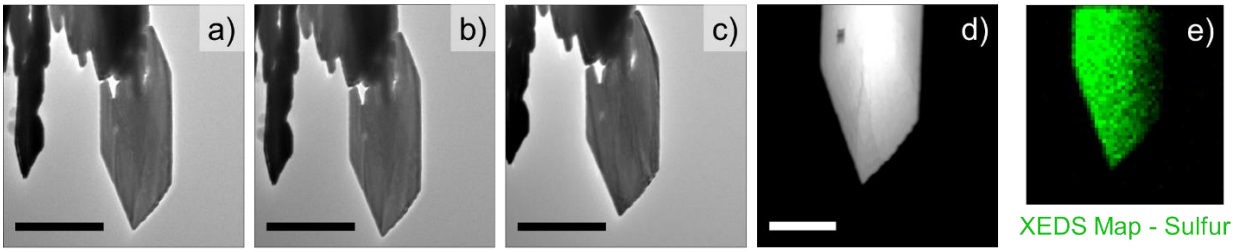

Figure 2. a) – c) Time series of images of a cryogenically cooled sulfur particle at approximately -173°C after **a)** 86 minutes, **b)** 170 minutes, and **c)** 311 minutes under 8.8×10^{-8} Torr vacuum. Scale bars 1 µm. The particle was not exposed to the electron beam between images. No sublimation effects were observed over a 5 hour period. After 4 hours under vacuum, a HAADF STEM image **(d)** (scale bar 500 nm) and STEM-XEDS map **(e)** were taken from the tip of the particle, demonstrating the stability of sulfur for STEM imaging and spectroscopic analysis under cryogenic conditions. Stronger signal on left hand side of particle due to detector geometry.

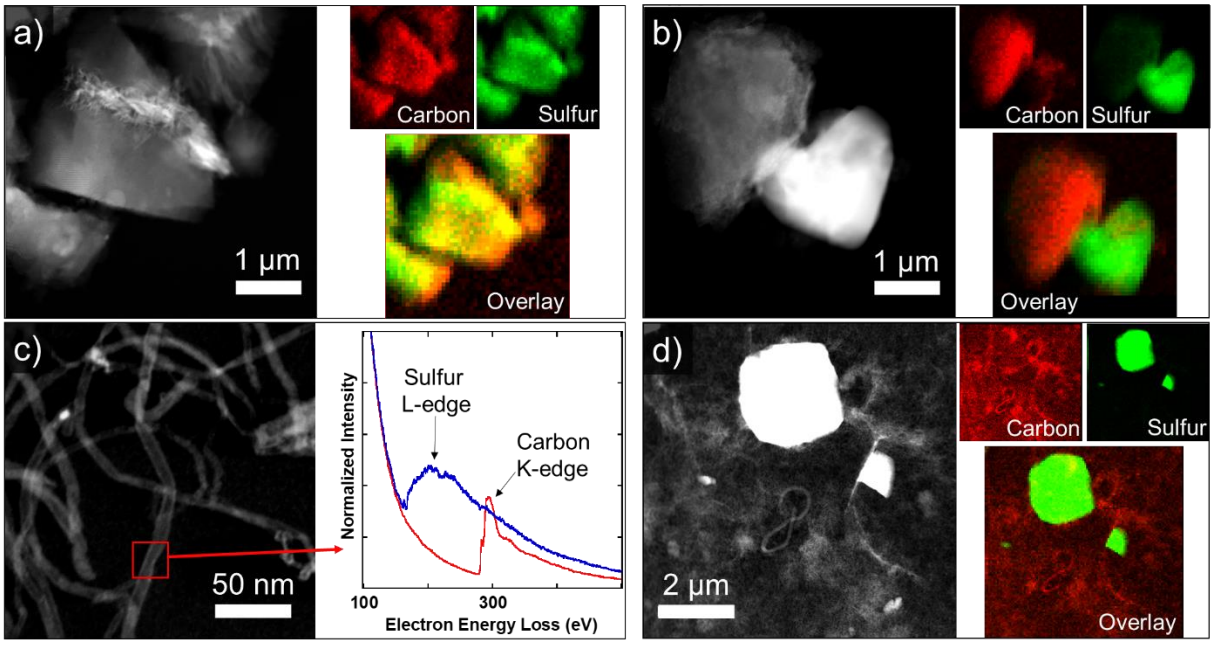

Figure 3. Cryo-STEM ADF images and XEDS maps of: **a)** Composite of sulfur and activated gyroidal mesoporous and microporous carbon aG^{D}MC-15-10h, showing a high degree and homogeneity of sulfur infiltration (overlap in carbon and sulfur signals). **b)** Composite of sulfur

and the same gyroidal mesoporous carbon G^{D}MC-15-1600°C without prior activation and very low microporosity, showing pure sulfur external to the carbon host, indicating poor infiltration efficiency. **c)** Cryo-STEM image of carbon nanotubes after attempted sulfur melt infusion. Tubes remain hollow. EELS spectrum from body of tube (red) on carbon support film shows little or no sulfur L-edge signal. EELS spectrum from an elemental sulfur particle shown for comparison in blue. **d)** Carbon nanotube-sulfur composite CNT-S, also showing most sulfur external to nanotubes.

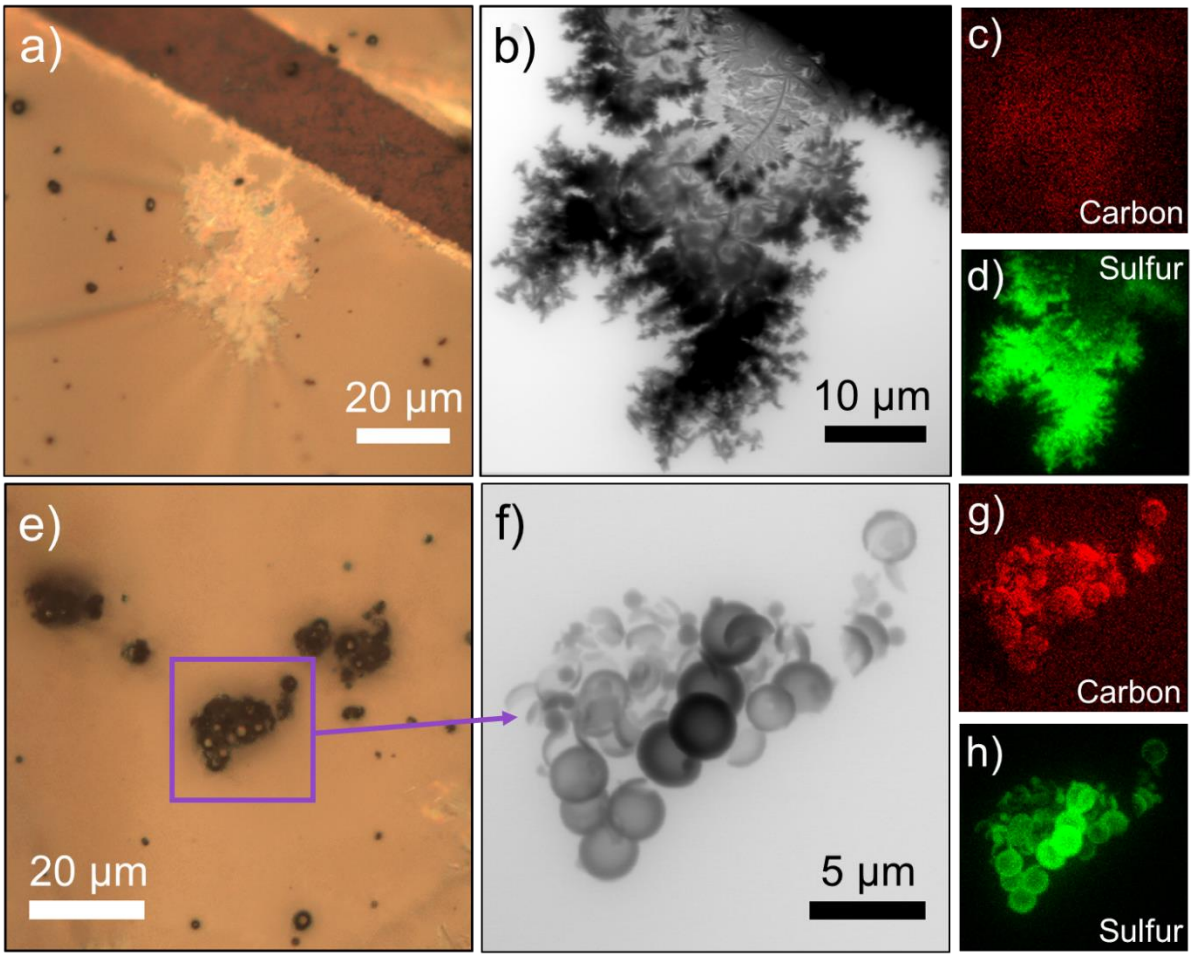

Figure 4. a) Optical microscope image of pure sulfur that has not infiltrated into carbon spheres. **b)** airSEM BF-STEM image of sulfur particle corresponding to that in the optical image. **c) & d)**

carbon and sulfur XEDS maps, confirming that the material is bulk sulfur. **e)** Extended depth of field optical microscope image of clusters of carbon-sulfur spheres recorded on the airSEM's optical microscope. **f)** airSEM BF-STEM image of single cluster of carbon spheres from the same region as (b). **g) & h)** XEDS maps showing carbon and sulfur signals that confirm sulfur infiltration into the sphere walls, but suggests no infiltration into the sphere interior.